Upscaled engineered functional microfibrillated cellulose flat sheet membranes for removing charged water pollutants

Journal:	*ACS Applied Materials & Interfaces*
Manuscript ID	am-2021-23285k
Manuscript Type:	Article
Date Submitted by the Author:	01-Dec-2021
Complete List of Authors:	Karim, Zoheb; MoRe Research Örnsköldsvik AB Georgouvelas, Dimitrios; Stockholm University, Environmental and Materials Chemistry Svedberg, Anna; MoRe Research Ornskoldsvik AB Monti, Susanna; National Research Council, Institute of Chemistry of Organometallic Compounds (ICCOM) Mathew, Aji; Stockholms Universitet, Department of Materials and Environmental Chemistry

Upscaled engineered functional microfibrillated cellulose flat sheet membranes for removing charged water pollutants

Zoheb Karim[1*], Dimitrios Georgouvelas[2], Anna Svedberg[1], Susanna Monti[3], Aji P Mathew[2]

[1]MoRe Research Örnsköldsvik AB, SE-891 22 Örnsköldsvik, Sweden

[2]Department of Materials and Environmental Chemistry, Stockholm University, SE-10691 Stockholm, Sweden

[3]CNR-ICCOM, Institute of Chemistry of Organometallic Compounds, via G. Moruzzi 1, I-56124 Pisa, Italy

Email: zoheb.karim@gmail.com

Phone: +46 764221267

Fax: +46 66075981

ABSTRACT

Polymeric composite membranes have shown great potential in removing pollutants from water. A significant limitation of polymeric membranes is the centimeter-sized dimensions, which limit their application at the pilot or industrial scales. In this study, flat sheet functional membranes of microfibrillated cellulose (MFC) with mixed and layered architectures are produced using the up-scaled Dynamic Sheet Former (Formette) in a fully water-based-system, and their potential for the removal of charged impurities from the aqueous medium is evaluated. The processing of composite membranes is unique in terms of size (1m × 20 cm), assembled MFC architectures, tunable porosity, functional groups densities, and free-standing at high water pressure. It is shown that the MFC assembly has a direct influence on the pollutant removal efficiency, and again the layered architecture turns out to be a more efficient scavenger of the charged pollutants due to the combined actions of electrostatic interactions, hydrogen bonding, and size exclusion. Experiments are supported by reactive molecular dynamics simulations that provide possible realistic scenarios at the atomic/molecular scale. All the data confirm the scalability and tunability of the MFC-based water cleaning membranes, which show high adsorption capacity, flexibility, hydrolytic stability, and mechanical robustness.

Keywords: Microfibrillated cellulose, Composite membranes, Metal ions removal, Functional adsorbents, MFC architectures, Computational chemistry

SYNOPSIS

Results of this article could be easily implemented for removing charged pollutants from water for an effective, sustainable water filter development.

INTRODUCTION

Among the different types of dangerous substances that are released in the environment, a considerable amount consists of charged metal ions and dyes, which usually come from industrial plants belonging to sectors such as mining, dyeing, electroplating, electrolysis, paper and pulp production, tanning, photography, metallurgy.[1,2] Conventional methods, such as chemical precipitation, filtration, ion exchange, electrochemical treatment, membrane technologies, adsorption on activated carbon, evaporation, etc., employed for the elimination of these pollutants from the industrial effluents[3,4] are inefficient, impractical, and insufficient to obtain substantial results. The removal of metal ions by chemical precipitation or electrochemical treatment is ineffective when the ions concentration is between 1-100 mg/L.[5], and the introduction of new undesirable chemicals (i.e. acids and bases for pH adjustment, flocculating chemicals, coagulants etc.) in the treated water is inevitable. Other conventional approaches like ion exchange, membrane technologies, activated carbon adsorption, or evaporation are costly primarily because of the large energy consumption.[6,7]

Nanocellulose, prepared through a top-down approach from wood biomass, and in particular, MFC, has shown high scavenging potential and thus been tuned for this purpose.[8-13] The MFC adsorption capacity and its capability to form stable networks when dried make it an excellent candidate for flat sheet composite membrane (FSCM) processing. As demonstrated in[14] MFC could be a useful, functional, and robust bio-based material in the field of water purification.

We are active in the production and application of sustainable bio-based membranes for water purification and focuses on comprehensive multi-disciplinary/scale investigations to understand the process-property-functional correlation and explore the assembly of these small particles within the produced dimensional architecture.[2,15-17]

Another big challenge is the up-scaling of the functional composite membranes without compromising the water flux, selectively, mechanical stability, pore-size distribution. To gain all these properties, Dynamic Sheet Former (Formette) was used for the production of MFC FSCMs at pilot/industrial scale.

Thus, his study focuses on (a) the production of FSCM as a prototype for an industrial scale water decentralization system, and (b) the assessment of the MFC assembled architecture (hybrid and layered) relative to the networking potential and the properties of the FSCM. The arrangement and self-assembly of MFC within (hybrid) and on (layered) long fibers networks have been exploited using sophisticated advanced techniques including atomistic molecular dynamics simulations based on a reactive force field (RMD). The potential use of the produced architectures as free-standing membranes for the separation of charged pollutants (metal ions and dyes) in aqueous media is demonstrated. All these aspects are fundamental in the field of

affinity membranes as next-generation bio-based membranes for water decentralization. The successful results indicate that the synergistic combination of all the experimental techniques and computational modeling can be used effectively for a thoughtful design of composite membranes with tuned separation capacity of charged impurities.

MATERIALS AND METHODS

High-grade MFC (Exilva P 01-V) was purchased from Borregaard AB (Sarpsborg, Norway). The pulp was supplied by MetsäBoard AB (Husum, Sweden). Dyes (Irgalite Blue RL (IB RL) and Irgalite Violet H (IV H)) were purchased from BASF Dispersions and Pigments, Germany, and industrial effluent contaminated with metal ions were collected from a cellulose production mil (paper and pulp industry) located in Sweden. All chemicals were in analytical grade and used without any further purifications.

Production of FSCM.

A complete water-based instrument,[14] Dynamic Sheet Former (Formette) was used for the production of MFC assembled flat sheet membranes, as mentioned in **Figure 1**. The 1:1 ratio of disintegrated (^{o}SR value 13.6) long pine fibers (0.5 wt%) and MFC (0.5 wt%,) is taken in the machine chest with continuous stirring and then pumped into a perforated cylinder (24×22 cm) through the nozzle (μm pore size). Hybrid suspension of long pine fibers and MFC was sprayed on wire mesh having 2000 cm^2 of surface area (20×100 cm). The drainage of the hybrid suspension was performed during the spinning of the perforated cylinder at a speed of 3000 rpm for 5 min. Semisolid flat sheet hybrid membrane was taken out carefully and dried further using a cylindrical dryer at a pressure of 100 kN at 90 ^{o}C for 2 min in a continuous mode having cylinder speed of 1 m/min. Likewise, for the production of the layered structure, first, long pine fibers (0.5 wt%) were sprayed on a wire mesh (base layer), and then the pristine MFC (0.5 wt%) was sprayed on the created base layer (**Figure 1)**.

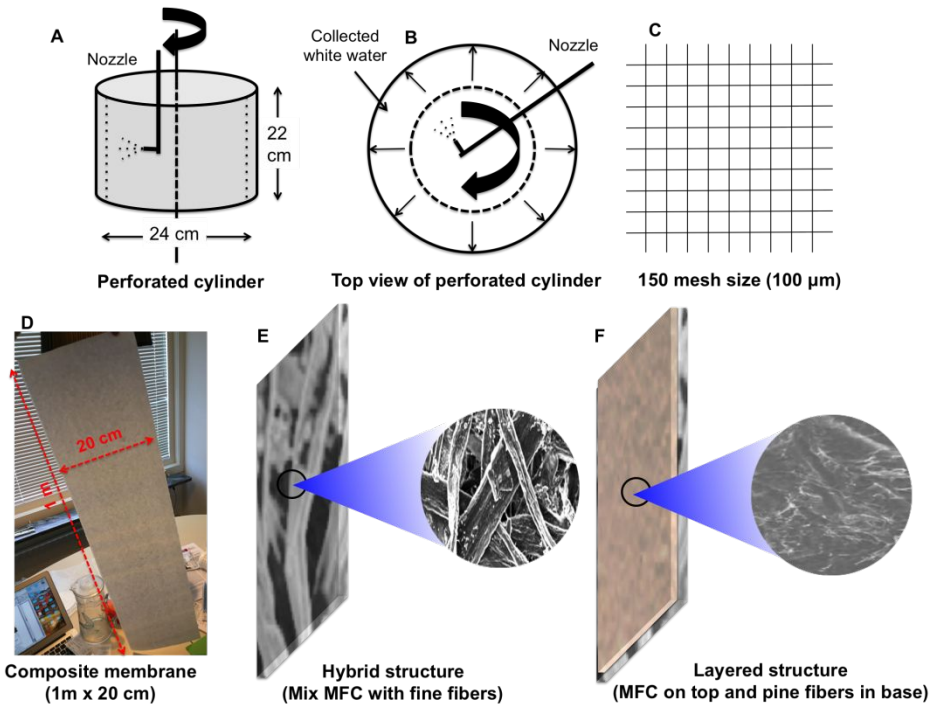

Figure 1. Diagrammatic representation of perforated cylinder (A) of dynamic sheet former used for the production of flat sheet membranes. Nozzle (B) used to spray the MFC and long pine fibers on wire mesh having 100 µm pore diameter (C). Spinning of the cylinder at 3000 rpm responsible for the drainage of water. Two types of self-assembled MFC architecture, hybrid (E) and layered (F) were produced, and fabricated MFC assembled membranes using dynamic sheet former is shown in (D).

CHARACTERIZATION

Mutek SZP 06, MUTEK was used for measuring the surface ζ-potential of the suspensions. Optical morphology of mix suspension (MFC and pine fibers) was obtained using Olympus Polarizing Microscopes (CX31-P). Nano/micro morphology of the composites membranes was captured using low-resolution Scanning Electron Microscope (SEM), JEOL, JSM-6010LV, (Japan). See **SI for details.** The pore-size distribution within composite membranes was measured using N_2 adsorption technique (BET) and Hg-porosimeter (AutoPore IV Micromeritics Instrument Corporation, USA). Porosity was further calculated manually with equation **S1**. Surface wettability tests were carried out using the sessile drop technique at room temperature. Mechanical properties of FSCM were measured with a tensile tester (Lorentzen & Wettre, ABB, Sweden) **(SI).** The water flux through the FSCM was measured using a Convergence Clean Water Flux (CWF) pilot system in continuous mode, at variable pressure, and given temperature (**Figure S2**).

REMOVAL OF CHARGED POLLUTANTS

Dyes. The Irgalite Blue RL and Irgalite Violet H dyes were selected to check the removal capacity of the produced FSCM. The combination of experiment and theory was used to explain possible behaviors of the dyes inside the filtration membranes

focusing on representative three-dimensional structures that were downloaded from the Cambridge Structural Database (IDs: CUPOCY10 and CEXNIC).[18,19] These were optimized at the quantum chemistry (QC) M06-2X/6-311G(d,p) level of theory in the gas phase using the Gaussian09 package (revision A02-)[20], and the final geometries were employed to estimate two relevant parameters that regulate the motion and morphology of the dyes, namely hydrated radius and radius of gyration. The hydrated radius was determined using the method proposed by Akbari and co-workers[21] by generating the solvent-accessible surface area (SASA) of each molecule with VMD[22] (spherical probe with a radius of 1.4 Å) and then calculating the equivalent spherical radius. Taking as reference data some of the values reported in **Table S1** of the SI of Akbari et al.[21] we used the correlation between the spherical and hydrated radii to estimate the unknown hydrated radius of the two dyes (**Table S1, Figure S3**). Some characteristics of the dyes are reported in **Table S2** and **Figure 5C**.

Metal ions. The industrial effluent collected from the pulp-producing industry, which contained various metal ions, was used for the removal study in cross-flow/dynamic mode. The effluent was first filtered with a Whatman filter paper 1 (cat. no. 1001090) to remove the bio-sludge, and then the filtrate was employed for the separation study. The metal ions present in the industrial effluent were Fe^{2+}/Fe^{3+}, Mg^{2+}, Cd^{2+}, Co^{2+}, Cr^{3+} and Mn^{2+} (**Figure 5A**). See details in SI**.** The measurement of dye and ions removal was calculated through Inductive Couple Plasma Atomic Emission Spectroscopy (ICP-OES) and UV-visible spectrophotometer(**equation S2**).

COMPUTATIONAL MOLECULAR MODELING

Model Building. Two different models were used to simulate adsorption and solvation of the carboxylated layered and hybrid membranes. The first one[23-26] consisted of sixteen aligned glucosyl chains, arranged as a parallelepiped rod with all the facets functionalized with carboxyl groups according to the experimental indications. The second one (hybrid model) was prepared by placing three fibers, one on top of the other (in the Z-direction) rotated by 60 degrees, in a simulation box where the initial size was 83.5×89.5×87.5 $Å^3$. (**Figure S4,** See details in SI).

Molecular Dynamics (MD) Simulations. The production MD simulations were performed in the NVT ensemble, and the system configurations were collected every 0.1 ps. Temperature and pressure were regulated through the Berendsen's thermostat and barostat with relaxation constants of 0.1 ps. The time step was set to 0.2 fs. The statistical analysis of the sampled data was carried out on the last three hundred configurations of the dynamics, considering atom-atom radial distribution functions (RDFs) and the percentage of surrounding species (in a 3.5 Å range). A possible arrangement of the membrane pores, pockets, tunnels,[28,29] positions of metal ions and solvent molecules was obtained examining the final configurations. This suggested possible adsorption trends in the two different architectures (**SI**).

RESULTS AND DISCUSSIONS

Processing. A complete water-based system, Dynamic Sheet Former (**Figure 1**), was used to produce the composite membranes.[2,14] The 150 wires mesh (100 μm pore diameter) perforated cylinder was not a clever approach for retention of 5-25 nm MFC, therefore, pine fibers (22-50 μm in diameter, 0.5 - 1.94 mm range in length and having surface ζ-potential of -11±24 mV) were introduced to obtain a stable three-dimensional network *via* hydrophobic/hydrophilic interactions. The loss of MFC during the fabrication of all the FSCM is shown in **Table 1**.

Physical properties. The thickness of dried reference, hybrid and layered membranes was 119, 94 and 97 μm, respectively, measured as mentioned in ISO 534. Both composite membranes have lower thicknesses compared to the reference. Densities at 50% relative humidity varied in the range of 550-702 kg/m^3, depending on the composition and preparation conditions. Assuming that the density of MFC was 1500 kg/m^3, the increased material density, compared with the 100% pine fiber reference membranes (550 kg/m^3), was related to the addition of MFC (**Table 1**). A high density of hybrid composite membranes (702 kg/m^3) was recorded even after the loss of 10.7 % MFC during processing, which could be explained by the decrease in porosity due to the packing of MFC in the pine fiber network. The obtained results were further supported by porosity calculation (**Table 1**).[10]

During the production of layered FSCM, the infusion of the MFC into the base layer (high load during drying, 100 kN) was observed (≈50 to 60 μm), thus, only the remaining 47 μm was represented by an open loose long pine fibers network, which might be responsible for the high porosity compared to the hybrid assembled MFC structure.[11,30] Hence, the studied up-scaled composite membranes are unique in the ways of their assembled MFC architectures, which could only and easily be achieved during processing on dynamic sheet former in a controlled manner. The assembly of MFC influences the final properties of the composite membranes and the removal of metal ions as discussed later.

Table 1: Physical properties of the produced flat sheet membranes.

Structures and their compositions	Grammage (g/m^2)		MFC loss (%)	Thickness (μm)	Porosity (%)	Density (kg/m^3)
	Targeted	Obtained				
Ref. structure (100%) PF	65	65	NA	119	48	550
100% PF in bottom and 100% MFC on top), 1 wt%	65 (55 BL and 10 TL)	65	0.00	97	32	616
Hybrid structure (1:1, PF and MFC), 1 wt%	65	58	10.7	94	29	702

PF = pine fibers, BL = base layer, TL = top layer, NA = not applicable

Morphological studies. The polarized micrographs of MFC shown in **Figure S1**, indicate that the fibers have nanometer/micrometer lengths and diameters of a few nanometers. [10-13]

Figure 2A shows a the produced FSCM. Cross-section of the flat sheet hybrid structure at low magnification (**Figure 2bi**), presented a tight network. In parallel, impregnation of the MFC within the porous dimensional network of pine fibers was undertaken to ensure that the surface functionality of MFC was readily accessible.[17] In a layered morphology (**Figure 2cii**), a top dense layer and bottom open structure were observed. The image indicates that the 100kN pressure applied during the drying of the layered flat sheet structure facilitated the infusion of the top layer into the open pine base network. Only 10g/m^2 grammage was targeted for the production of the top layer, which might not be enough for the production of dual-layered morphologies, but it could be achieved when low pressure (60 kN), and 1 wt% of cellulosic nanofibers was used in the fabrication process.[16] The processed membranes using pilot-scale dynamic sheet former could have some unique morphological characteristics like the alignment of fibers towards the spin direction, which could not be achieved using the lab base vacuum-filtration approach. We have also noted that the water content (moisture) during the processing of membranes could also be controlled easily during spinning.

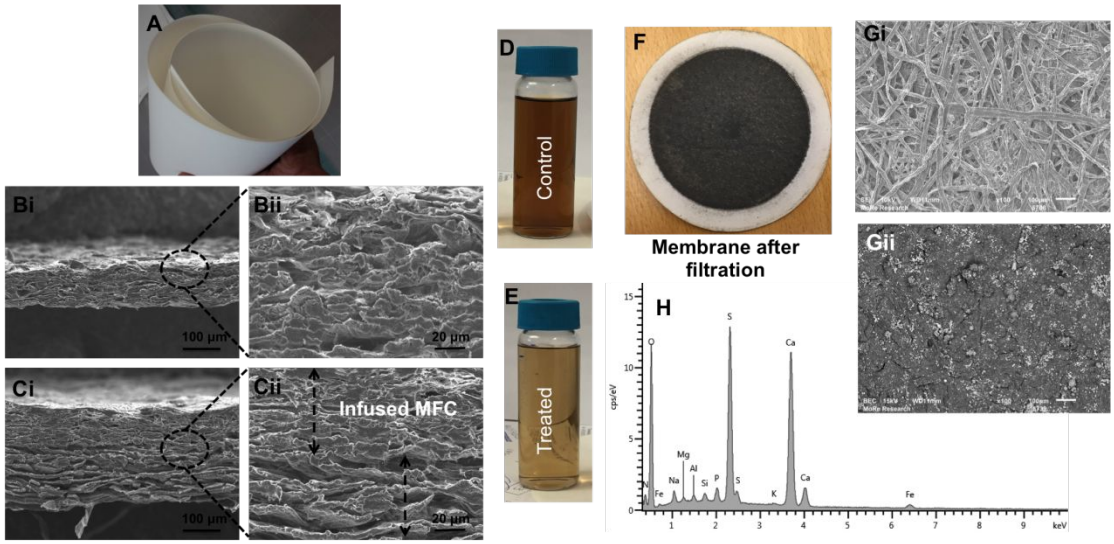

Figure 2: Visual expression (A) and SEM analysis of produced flat sheet membranes. Hybrid flat sheet membranes in low (Bi) and high (Bii) resolution are shown. Cross- morphology of layered FSCM (Ci and Cii). For detailed morphology, see supplementary **Figure S5.** Furthermore, the removal experiment of metal ions in cross-flow mode is shown. (D) and (E) represent the untreated and treated industrial effluent, respectively. A flat sheet membrane after industrial effluent filtration is shown in (F). SEM images of used membranes before (Gi) and after (Gii) effluent filtration and finally EDS spectrum of attached Mg^{2+} ions on the surface of used flat sheet composite membranes (H).

Mechanical performance. Mechanical properties of the produced membranes were analyzed in two directions (**Table 2**). We were expecting the alignment of fibers towards the spin direction (SD). The tensile strength of the reference sample in SD

was 21.2 MPa, but ≈1.2 fold decrease in strength was calculated in the cross direction (CD), and a similar trend was noticed for both FSCM (**Table 2**).[11,31]
Here, membrane drying was performed in continuous mode on a moving cylinder, which gives a uniform heating effect for the formation of hydrogen bonds and mechanical stability to the membranes. The high surface area of MFCs increases the fiber-fiber interaction giving a highly consolidated structure with high tensile strength and toughness compared to the reference membranes.[32-34] The mechanical properties of the composite membranes were also recorded in wet conditions. The results followed the same trends as the dry composite membranes, but lower values were reported.[15,16]

Table 2: Mechanical properties of produced membranes in dry and wet conditions

Structures		Tensile strength (MPa)		Strain at break (%)		E-modulus (MPa)	
		SD	CD	SD	CD	SD	CD
Dry	Reference (PF)	21.2±0.3	17.5±0.2	2.6±0.8	2.6±0.4	292±2.8	221±2.6
	Layered structure	33.1±0.2	28.0±0.7	1.4±0.5	1.4±0.5	330±1.7	280±3.4
	Hybrid structure	65.7±0.9	49.1±0.1	1.5±0.2	1.4±0.7	350±2.4	310±3.1
Wet	Reference (PF)	0.32±0.05	0.21±0.08	0.54±0.07	0.47±0.4	201±0.2	197±0.2
	Layered structure	0.73±0.06	0.56±0.04	0.27±0.08	0.28±0.4	324±0.9	289±0.7
	Hybrid structure	1.9±0.04	0.82±0.03	0.31±0.05	0.34±0.8	346±0.7	302±0.9

SD = spin direction, CD = cross direction

Pore-size distributions and water flux. A broad distribution of pore sizes and a high pore volume were detected for the reference membrane (**Figure S6a**). The maximum pore volume was in the range of 55-150 nm, which indicates macropores (> 50 nm). After the introduction of MFC (10 g/m^2), a decrease in the pore size distribution and volume was detected. A drastic shift of the pore diameter and volume from 150 nm to 78 nm and 1 nm to 0.03 nm, respectively, was observed (**Figure S6b)**. The maximum distribution of the pores in the layered FSCM was found in the range of mesopores (2-50 nm). In the case of the hybrid FSCM, a pore size distribution (1 nm to 65 nm) lower than the reference and layered composite membranes was present.[14]
Due to the pores distribution range limitation, (<1 nm to 150 nm) of N_2 gas adsorption technique (BET), Hg-porosimetry (pore-range, 5 nm-1 mm) was carried out. The open pores in the reference membranes were in the range of 3 to 10.7 μm, and the maximum pore volume was in the range of 4 to 7 μm.[15]

At a pressure of 0.5-1.5 bars, the water flux of all membranes was increased with respect to applied pressure. The highest water flux was reported for the reference membrane, followed by layered and hybrid flat sheet structures. The water flux of the reference at 1.5 bar was 9625 L/m^{2}h, which further decreased to 7000 L/m^{2}h for the layered flat sheet membranes, and the lowest flux was recorded for the hybrid flat sheet structures (6750 L/m^{2}h) (**Figure S6d**). A very thin infused layer of MFC (≈50 μm) was produced during the processing of the flat sheet layered membrane. This infused layer does not have any drastic hindrance forces for the free water flow and no significant decrease in the water flux was recorded. Thus, an ultrahigh water flow through the layered flat-sheet membranes could be due to the nanochannels inside the assembled MFC network as reported by Ma et al. and others..[16,35,36]

Membranes performance for pollutants removal. All six cationic metal ions targeted in this study are listed in **Table 3**. A very low removal percentage (1 to 3%) and removal capacity in the range of 0.7-1.2 mg/g of all the metal ions was recorded using the reference membranes. The highest removal (98%) was obtained with the layered FSCM for the Mn^{2+} ions followed by Cd^{2+}. The whole removal percentage was in the order: $Mn^{2+} > Cd^{2+} > Mg^{2+} > Cr^{3+} > Fe^{2+}/Fe^{3+} > Co^{2+}$ and the removal capacity in the order: $Mg^{2+} > Mn^{2+} > Cd^{2+} > Fe^{2+}/Fe^{3+} > Cr^{3+} > Co^{2+}$, indeed, the removal capacity is a quantitative analysis that depends on the initial concentration of the individual metal ions.[1,37-39]

In the case of layered assembled MFC membranes, a low contact angle is recorded due to the low density of carboxylic functional groups, increasing the hydrophilic character of the surface, which improves the immobilization capacity of the charged pollutants compared to the hybrid membranes.[11,12,39]

Table 3: Removal experiment of industrial effluent in cross-flow mode

Name of metal ions	C_o (μ g/L)	C_t (μ g/L)		Removal (%)		Removal capacity (mg/g)	
		LCM	HCM	LCM	HCM	LCM	HCM
Fe^{2+}/Fe^{3+}	616	244±0.029	341±1.10	60	44	157	142
Mg^{2+}	5800	1070±0.13	3350±0.42	81	42	737	717
Cd^{2+}	5.77	0.292±0.05	0.757±0.12	94	86	194	201
Co^{2+}	1.03	0.533±0.12	0.864±0.20	48	16	59	51
Cr^{3+}	9.87	3.32±0.65	7.55±1.95	66	23	64	67
Mn^{2+}	342	4.95±1.50	8.97±0.80	98	97	223	201

LCM = Layered composite membrane, HCM = Hybrid composite membrane

It was found that, despite the low charge density (48.45±4 μmole/g) and surface ζ -potential (-38±2.2 mV) of MFC, both composite membranes had a high removal capacity of all the metal ions. This is also evident from the analysis of the simulations

results that identified possible capture mechanisms in the two architectures from the RDFs and the cellulosic matrix pores and channels. In the layered system, where a narrow canal filled with solvent separates the fibers (periodic representations), the solvated glucosyl chains maintained an ordered orientation, and their packing arrangement was almost preserved. A mild swelling was caused by the inner adsorption of a few water molecules and hydrogen bonds with the first water shell (within 3.5 Å), which contained approximately 43% of the surrounding waters. The carboxyl functional groups, which were randomly distributed on all four fiber sides, could be involved in interchain interactions, but most of the time, they were deprotonated (80%) and pointed towards the solvent. This favored the capture of the metal cations, as suggested by the trends displayed in **Figure S7**.

The presence of relatively sharp peaks at short distances in all the X-O(WAT) RDFs suggests that all the ions were surrounded by water and could be found in solution or close to the surface, still coordinated with a few water molecules. The Cr ions were located preferentially in the middle of the channel or close (within 3.5 Å) to the cellulose hydroxyl (12%) but far from the carboxyl oxygens that were, instead, the target of the other two ions types, namely Fe and Mg. Indeed, 47% of the Fe ions were connected to the carboxyl chains, as indicated by the two peaks at short Fe-O(COO^-) distances (2.1 and 3.0 Å). These peaks evidence the presence of Fe_2O_3•$3H_2O$ species that is further confirmed by the sharp peak centered at about 3 Å in the Fe-Fe RDF profile displayed in **Figure S8**. On the contrary, only 7% of the Fe ions interacted with the other oxygens of the fibers. Mg ions were also connected to the carboxyl groups (20%) but located farther from the other cellulose oxygens (2% within 3.5 Å). Furthermore, all the metal ions remained far from each other (at separations greater than 5.5 Å).

The scenario is entirely different in the hybrid system. There, the ordering of the chains was partially disrupted, and the carboxyl groups were randomly distributed inside the cellulose matrix. The deprotonation of these moieties was reduced (60%), and the cellulose water content increased in relation to the other system (92% of the water molecules, instead of 80%, were found within 3.5 Å of the cellulose atoms). The matrix showed a highly porous structure with big pockets, tunnels, and cavities that could host water and ions. Depending on the local character (that is on the group forming these areas), metal ions could remain entrapped, indirectly interact with other metal ions, and hardly be released by the membrane. Possible interaction schemes and pores structures were obtained by examining the RDF profiles of **Figures 3a-c** and the membrane sections shown in **Figures 3d,e** and **S9**.

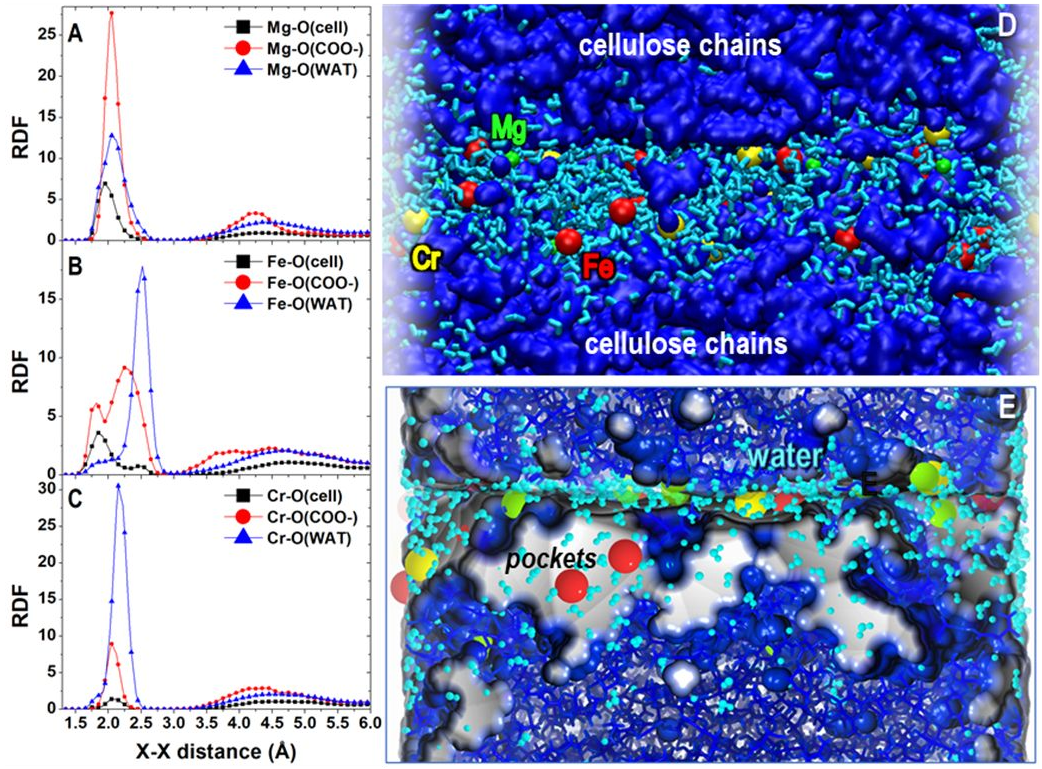

Figure 3. **A**, **B**, **C**) Radial distribution functions (RDFs), obtained from the final portions of the MD trajectories of the hybrid membrane model, between the metal ions and the cellulose oxygens not including the carboxyl ones [O(cell)], the carboxyl oxygens [O(COO-)] and water oxygens [O(WAT)]. **D**, **E**) Snapshot extracted from the final stage of the MD simulations. This magnification represents a section of the simulation box (parallel to the XZ plane) where pockets filled with water and ions are highlighted (solid blue-grey spheres) in **E**. In **D**, the cellulose chains are rendered through a solid blue solvent accessible surface, whereas blue sticks are used in **E**; the ions are depicted as red (Fe), yellow (Cr), and green (Mg) spheres; water molecules are cyan sticks. **D**) VMD visualization of a XZ section of the membrane and its corresponding CAVER representation with small and big pockets (**E**). Other perspective views are shown in **Figure S9** of the SI.

The sharp and broad red peaks at short distances in all the X-O(COO^-) RDFs suggest that all the ions could directly interact with the carboxyl oxygens and sit at closer distances in a range of 1.8 - 2.2 Å. This indicates, again, given the two peaks in the Fe-O(COO^-) and Fe-O(cell) RDF plots and in the Fe-Fe distance profile of Figure SM5, the presence of Fe_2O_3 species. The percentage population of the ions-cellulose connections in this hybrid organization of the chains is more balanced than in the layered model, being 41%, 45%, and 14% for Fe, Mg, and Cr, respectively, but in line with the previous trend of Cr ions. In fact, interactions between Cr and the cellulose oxygen atoms are weak, probably because of the competitive interactions with the other species. Only 28% of the Cr ions were located within 3.5 Å of the cellulose hydroxyls, whereas Fe and Mg had stronger interactions as confirmed by their percentage populations, namely 75% and 78% for Fe and Mg, respectively. Water molecules always surrounded the ions that could also be placed close to each other due to relatively strong immobilization and entrapment in narrow regions, as is evident in the RDF plots shown in **Figure S9** and in the membrane sections shown in **Figures 3e,f**.

From an experimental point of view, it could be hypothesized that a combination of adsorption, aggregation into bigger nanoparticles, and subsequent size-exclusion could be the separation mechanism of metal ions from industrial effluent (**Figure S10**). It was reported earlier that functional membranes prepared using cellulose nanofibers with vacuum filtration, having an average pore diameter of 194 Å and a few active groups on the surface, adopt a similar mechanism for removing the metal ions.[15,40,41]

The design of flat sheet composite membranes is also crucial. During the production of the layered composite membranes, we sprayed MFCs on top of the pine base layer, to tune both the pore size and structure of this region. We obtained a film that could be easily seen by inspection of the SEM analysis (**Figure 2ci and 2cii**). This modulated self-assembled architecture is essentially a sieve with finely arranged narrow channels that could be controlled through the regulation of the top layer.[42-44] This is very effective for a fast immobilization of a large number of metal ions.

The removal capacity of metal ions was further compared with cellulose/nanocellulose and its derivatives, as reported in the literature. In the case of ferric ions (Fe^{3+}), Q_{max} was 115[1] and 19 mg/g[45] for functionalized nanocellulose and cellulose, respectively, and both values are lower in relation to those found in the current study, which are 157 and 142 mg/g of removal capacity for the layered and hybrid MFC assembled composite membranes, respectively. A high removal capacity (335 mg/g) for Cd^{2+} was reported by Yu et al. 2013[46] using modified cellulose (carboxylated cellulose). In another report, polymer grafting was performed to attach amino groups on the surface of MFC, and surprisingly a low removal capacity (179 mg/g) was calculated.[38] Here, Cd^{2+} removal capacity was 201 mg/g of the used hybrid composite membranes. In an article[37] TEMPO-oxidized functionalized cellulose nanofibers used for the adsorption of Cr(III) at pH of 6.2 - 6.5, showed an adsorption capacity of 58 mg/g, which is lower than the one measured here.[37] It might be interesting to note that only the 10^{th} pass of the industrial effluent was performed through composite membranes. Thus the reported values are not for the saturation limit. In parallel, all values reported in the literature denote the saturation limit (Q_{max} values).

Separation of dyes impurities in cross-flow mode. The 80% removal of IV H dye was recorded using the layered FSCM, as shown in **Table S3**. The removal percentage of IV H was further increased when a hybrid flat sheet membrane was used, and reached 82%. A significant increase in percentage removal from 71% to 83% of IB RL, with respect to the layer and hybrid FSCM, was recorded, (**Table S3, Figure 4**). In a previous study[2], the highest removal of 88 to 98% was found for Victoria Blue 2B It is worth mentioning that bulk adsorption and ultrafast removal in a dynamic mode made this approach more suitable and adequate for the industrial-scale setup.

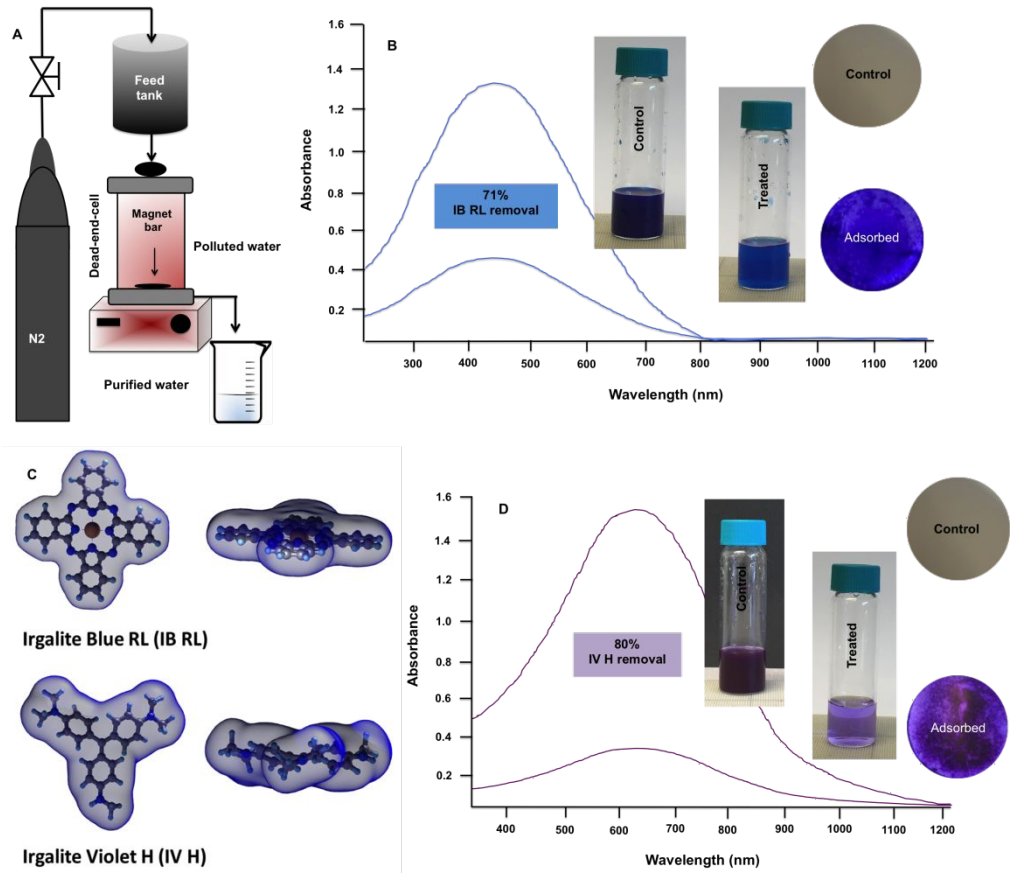

Figure 4. Removal experiment of dyes using the produced flat sheet composite membranes in cross-flow mode (A). The spectrum of Irgalite Blue RL was recorded at 449 nm (B). Irgalite Violet H visible spectrum is shown in (D), the spectrum was captured at a wavelength of 652 nm (λ_{max}). The removal percentage was calculated as reported in equation (ii). A decrease in color intensity after separation can be easily seen. Furthermore, a change in color after filtration of the dyes solution confirmed the adsorption of the dye molecules on the surface of the composite membranes. Finally, optimized molecular structures of the two dyes (balls and sticks models) are shown (C).

The effect of the charge and hydrodynamic/hydrated radius of the dyes on the retention of the surface of the membranes or inside their pockets and tunnels could be evaluated considering long-distance interactions, local character of the nanocellulose networks, and specific assembly of the fibers. The negatively charged functional groups of the chains imparted to the whole texture a negatively charged nature and thus the ability to attract positively charged ions. The intensity of this driving force was mitigated by the random distribution of the head groups on the fiber surfaces, their local density, and the presence of other moieties that could reduce their action through intramolecular hydrogen bonds. Indeed, after attraction and adsorption on the surface of the fibers, the dyes could remain entrapped in local pockets or channels inside the network and be kept there by the concerted action of the local moieties, namely carboxyl, hydroxyl, and epoxy groups present in the cellulose chains. It might be speculated that high retention of the dyes is obtained by favorable cooperative interactions, including charge neutralization and hydrophobic interactions of their rings with the hydrophobic portion of the cellulose chains. It was also observed that

the selected dyes, which contain several conjugated rings, are quite rigid and have the tendency to form molecular aggregates where the molecules can adopt stacked and T-shape arrangements. This determined an increase in the hydrated radius and thus enhanced retention.

The adsorption of charged pollutants via available functional groups has been reported extensively in the literature,[42,47-50] and a similar phenomenon (**Figure S10)** is also responsible for the removal mechanism of metal ions and dyes, whereas size-exclusion becomes dominant afterward.

OUTLINE

We have reported a fully water-based system for the up-scaling of MFC FSCMs (0.2 × 1 m). A Dynamic sheet former, a unique membrane processing device, is used to produce two assembled architectures with a controlled congregation of MFC within a long pine fibrous network (hybrid) and on top of it (layered). The assembly of MFC has a direct influence on the final properties of membranes, such as ultrahigh water permeability and open fibrous networks (layered membranes). Pilot-scale processing of the membranes imparted extraordinary properties, like the orientation of fibers in the spin direction of the machine (high tensile strength in spin direction), controlled infusion of MFC within lone pine fibrous based layer, uniform pore-size structures, and distribution, and tunable surface properties, which could be challenging to achieve using a lab-based vacuum-filtration approach.[11] The up-scaled membranes were used for the adsorption of dyes and metal ions from model and industrial water. Both membranes showed effective removal of both the targeted metal ions and the positively charged dyes. The available $-OH^-$ and $-COO^-$ functional groups on the membrane's surface were responsible for the binding of metal ions. In the case of the layered type, the ultrafast adsorption followed by the entrapment of the metal ions in locations nearby caused the formation of metal clusters, which narrowed the channel thus increasing the percentage removal.

It might be interesting to use this proposed fully water-based system for the continuous production of membranes for real module design. Large volume filtration of industrial effluent contaminated with various types of pollutants and study on the selectivity of pollutants towards grafted functional groups could be the future aim.

AUTHORS' CONTRIBUTIONS

All work was carried out under the supervision of ZK. ZK carried out most of experiments and analyzed, summarized and explained all the obtained results in the article. DG performed flux measurement and pore-size distribution experiments, and also contributing in writing the article. AS review the article. APM improved the manuscript respect to journal standard. SM carried out all computational studies. All authors read and approved the final manuscript.

ACKNOWLEDGEMENT

We are deeply grateful to Elly Westberg, MoRe Research Örnskoldsvik AB, Sweden for zeta-potential measurement. Marie Tjärnström, Jessica Sjöstedt and Pia Renström

were highly acknowledged for low resolution SEM, optical microscopy and mechanical properties measurements, respectively. SM is grateful to the CINECA Supercomputing Center for computational support (ISCRA program).

FUNDING

MistraTerraClean (Project number 2015/31) is high acknowledged for financial support.

CONFLICT OF INTEREST

No conflict of interest has been reported.

REFERENCES

(1) Liu, P., Borrell, P.F., Bozic, M., Kokol V., Oksman K. Nanocellulose and their phosphorylated derivatives for selective adsorption of Ag^{2+}, Cu^{2+} and Fe^{3+} form industrial effluents. *J. Hazard. Mat.* **2015**, 294, 177-185.

(2) Karim, Z., Mathew, A. P., Grahn, M., Mouzon, J., Oksman, K. Nanoporous membranes with cellulose nanocrystals as functional entity in chitosan: removal of dyes from water. *Carbohy. Poly.* **2014**, 112, 668-676.

(3) Volesky, B. Detoxification of metal-bearing effluents: biosorption for the next century, *Hydrometallurgy*, **2001**, 59, 203–216.

(4) Wang, J., Chen, C. Biosorption of heavy metals by Saccharomyces cerevisiae: a review, *Biotecnol. Adv.* **2006**, 24, 427–451.

(5) Wang, Z., Zhang, W., Yu, J., Zhang, L., Liu, L., Zhou, X. Fan, Y. Preparation of nanocellulose/filter paper (NC/FP) composite membranes for high-performance filtration. *Cellulose*, 2019, 26, 1183-1194.

(6) Mututuvari, T.M., Tran, C.D. Synergistic adsorption of heavy metal ions and organic pollutants by supramolecular polysaccharide composite materials from cellulose, chitosan and crown ether, *J. Hazard. Mat.* **2013**, 264, 449-459.

(7) Qu, X., Alvarez, P.J.J., Li, Q. Applications of nanotechnology in water and wastewater treatment. *Water Res.* **2013**, 47, 3931–3946.

(8) Ogeda, T.L., Silva, I.B., Fidale, L.C., EI-Seoud, A.O., Petri, D.F.S. Effect of cellulose physical characteristics, especially the water sorption value, on the efficiency of its hydrolysis catalyzed by free or immobilized cellulose. *J. Biotechnol.* **2012**, 157, 246-252.

(9) Melvin, H.K., Leo, C.P. The coherence between TiO_2 nanoparticles and microfibrillated cellulose in thin film for enhanced dispersal and photodegradation of dye, *Prog. Org. Coat.* **2019**, 132, 70-75.

(10) Castro, D.O., Karim, Z., Medina, l., Haggstrom, J.O., Carosio, F., Svedberg, A., Wagberg, L., Soderberg D, Berglund, L. A. The use of a pilot-scale continuous paper process for fire retardant cellulose-kaolinite nanocomposites. *Comp. Sci. Technol.* **2018**, 162**,** 215-225.

(11) Karim, Z., Svedberg, A., Lee, K.Y., Khan, M.J. Processing-structure-property correlation understanding of microfibrillated cellulose based dimensional structures for ferric ions removal. *Sci. Rept.* **2019**, 9, 10277.

(12) Karim, Z., Monti, S., Barcaro, G., Svedberg, A., Ansari, M.A., Afrin, A. Enhanced sieving of cellulosic microfibers membranes via tuning of interlayer spacing. *Environ. Sci.: Nano*, **2020**, 7, 2941.

(13) Onwumere, J., Piatek, J., Budnyak, T.M., Chen, J., Budnyk, S., Karim, Z., Thersleff, T., Kustrowski, P., Mathew, A.P., Slabon, A. CellPhot: Hybrid cellulose-bismuth oxybromide membranes for pollutants removal, *ACS App. Mat. Inter.* **2020***,* 12, 42891/42901.

(14) Karim, Z., Svedberg, A. Controlled retention and drainage of microfibrillated cellulose in continuous paper production. New J. Chem. **2020**, 44, 13796-13806.

(15) Karim, Z., Claudpierre, S., Grahn, M., Oksman, K., Mathew, A. P. Nanocellulose based functional membranes for water cleaning: Tailoring of mechanical properties, porosity and metal ion capture. *J. Memb. Sci.* **2016**, 514, 418-428.

(16) Karim, Z., Mathew, A. P., Kokol, V., Wei, J., Grahn, M. High-flux affinity membranes based on cellulose nanocomposites for removal of heavy metal ions from industrial effluents. *RSC Advances,* **2016**, 6, 20644-20653.

(17) Mautner, A., Maples, H.A., Kobkeatthawin, V., Kokol, Z., Karim, Z., Li, K., Bismark, A. Phosphorylated nanocellulose papers for copper adsorption from aqueous solutions. *Int. J. Environ. Sci. Technol.* **2016**, 13, 1861-1872.

(18) Brown C. J. Crystal structure of β-copper phthalocyanine. *J. Chem. Soc. A: Inorg. Phy. Theo.* **1968**, 2488-2493.

(19) Lovell S., Marquardt B. J., Kahr B. Crystal violet's shoulder" *J. Chem. Soc. Perkin Trans.* **1999**, 2, 2241-2247.

(20) Frisch, M.J., Trucks, G.W., Schlegel, H.B., Scuseria, G.E., Robb, M.A., Cheeseman, J.R., Scalmani, G., Barone, V., Mennucci, B., Petersson, G.A., Nakatsuji, H., Caricato, M., Li, X., Hratchian, H.P., Izmaylov, A.F., Bloino, J., Zheng, G., Sonnenberg, J.L., Hada, M., Ehara, M., Toyota, K., Fukuda, R.J., Ishida, T., Nakajima, Y., Honda, O., Kitao, H., Nakai, T., Vreven, J.A., Montgomery Jr, J.E., Peralta, F., Ogliaro, M., Bearpark, J.J., Heyd, E., Brothers, K.N., Kudin, V.N., Staroverov, R., Kobayashi, J., Normand, K., Raghavachari, A., Rendell, J.C., Burant, S.S., Iyengar, J., Tomasi, M., Cossi, N., Rega, J.M., Millam, M., Klene, J.E., Knox, J.B., Cross, V., Bakken, C., Adamo, J., Jaramillo, R., Gomperts, R.E., Stratmann, O., Yazyev, A.J., Austin, R., Cammi, C., Pomelli, J.W., Ochterski, R.L., Martin, K., Morokuma, V.G., Zakrzewski, G.A., Voth, P., Salvador, J.J., Dannenberg, S., Dapprich, A.D., Daniels, O., Farkas, J.B., Foresman, J.V., Ortiz, J., Cioslowski D.J. Fox, Gaussian 09, Revision A.02, Gaussian Inc., Wallingford CT, 2009.

(21) Akbari, A., Sheath, P., Martin, VD., Shinde, B., Shaibani, M., Banerjee, P.C., Tkacz, R., Bhattacharyya D., Majumder, M. Large-area grapheme based nanofiltration membranes by shear alignments of discotic nematic liquid crystals of grapheme oxide. *Nat. Comm.* **2016**, 7, 10891.

(22) Humphrey, W., Dalke, A. and Schulten, K. VMD - Visual Molecular Dynamics, *J. Mol. Grap.* **1996**, 14, 33-38.

(23) Zhu, C., Monti, S., Mathew, A.P. Evaluation of nanocellulose interactions with water pollutants using nanocellulose colloidal probes and molecular dynamic simulations. *Carbohy. Poly.* **2020**, 229, 115510.

(24) Valencia L., Nomena E. M., Monti S., Rosas-Arbelaez W., Mathew A. P., Kumar S., Velikov K. P. Multivalent ion-induced re-entrant transition of carboxylated cellulose nanofibrils and its influence on nanomaterials' properties, *Nanoscale*, **2020**, 12, 15652-15662.

(25) Valencia L., Monti S., Kumar S., Zhu C., P. Liu, S. Yu, A. P. Mathew. Nanocellulose/graphene oxide layered membranes: elucidating their behavior during filtration of water and metal ions in real time. *Nanoscale*, **2019**, 11, 22413-22422.

(26) Zhu C., Monti S., Mathew A. P. Cellulose. Nanofiber–Graphene Oxide biohybrids: disclosing the self-assembly and copper-ion adsorption using advanced microscopy and ReaxFF simulations, *ACS Nano,* **2018**, 12, 7028-7038.

(27) Plimpton, S. Fast parallel algorithms for short-range molecular dynamics, *J. Comp. Phy.***1995**, 117, 1-19.

(28) Aktulga, H.M., Fogarty, J C., Pandit, S.A., Grama A.Y. Parallel reactive molecular dynamics: Numerical methods and algorithmic techniques. *Parallel Comp.* **2012**, 38, 245-259.

(29) Jurcik, A., Bednar, D., Byska, J., Marques, S. M., Furmanova, K., Daniel, L., Kokkonen, P., Brezovsky, J., Strnad, O., Stourac, J., Pavelka, A., Manak, M., Damborsky, J., Kozlikova, B. CAVER Analyst 2.0: Analysis and Visualization of Channels and Tunnels in Protein Structures and Molecular Dynamics Trajectories, *Bioinformatics*, bty 386, **2018**.

(30) Mair, C. Control of porous structure of paper in a continuous process, Master thesis, KTH Royal Institute of Technology, Stockholm, Sweden, **2016**.

(31) Ma, H., Burger, C., Hsiao, B. S., Chu, B. Ultrafine polysaccharide nanofibrous membrane for water purification. *Biomacromolecules,* **2011**, 12, 970-976.

(32) Prakobna, K., Berthold, F., Medina, L., Berglund, L. A. Mechanical performance and architecture of biocomposite honeycombs and foam from core-shell halocellulose nanofibers. *Comp. Part A*. **2016**, 88, 116-122.

(33) Henriksson, M., Berglund, L. A., Isaksson, P., Lindström, T., Nishino, T. Cellulose nanopaper structures of high toughness. *Biomacromolrcules,* **2008**, 9, 1579-1585.

(34) Wang, Z., Niing, A., Xie, P., Gao, G., Xie, L., Li, X., Song, A. Synthesis and swelling behaviors of carboxymethyl cellulose-based superabsorbent resin hybridized with graphene oxide. *Carbohy. Poly.* **2017**, 157, 48-56.

(35) Ma, H., Burger, C., Hsiao, B.S., Chu, B. Highly permeable polymer membranes containing directed channels for water purification, *ACS Macro Lett.* **2012**, 1, 723–726.

(36) Goetz, L.A., Jalvo, B., Rosal, R., Mathew, A.P. Superhydrophilic antifouling electrospun cellulose acetate membranes coated with chitin nanocrystals for water filtration. *J. Memb. Sci.* **2016**, 510, 238-248.

(37) Sehaqui, H., de Larraya, U.P., Liu, P., Pfenninger, N., Mathew, A.P., Zimmermann, T., Tingaut, P. Enhancing adsorption of heavy metal ions onto biobased nanofibers from waste pulp residues for application in wastewater treatment. *Cellulose*, **2014**, 21, 2831–2844.

(38) Hokkanen, S., Repo, E., Suopajärvi, T., Liimatainen, H., Niinimaa, J., Sillanpää, M. Adsorption of Ni(II), Cu(II) and Cd(II) from aqueous solutions by amino modified nanostructured microfibrillated cellulose. *Cellulose*, **2014**, 21, 1471–1487.

(39) Liu, P., Sehaqui, H., Tingaut, P., Wichser, A., Oksman, k, Mathew, A.P. Cellulose and chitin nanomaterials for capturing silver ions (Ag^{2+}) form water via surface adsorption. *Cellulose*, **2014**, 21, 449-461.

(40) Maneerung, T., Tokura, S., Rujiravanit, R. Impregnation of silver nanoparticles into bacterial cellulose for antimicrobial wound dressing, *Carbohh. Poly.* **2008**, 72, 43-51.

(41) He, J.H., Kunitake, T., Nakao, A. Facile in-situ synthesis of noble metal nano-particles in porous cellulose fibers. *Chem. Mat.* **2003**, 15, 4401–4406.

(42) Saito, T., Isogai, A. Ion-exchange behavior of carboxylate groups in fibrous cellulose oxidized by the TEMPO-mediated system, *Carbohy. Poly.* **2005**, 61,183–190.

(43) Mianehrow, H., Afshari, R., Mazinani, S., Sharif, F., Abdouss, M. Introduction a highly dispersed reduced graphene oxide nanobiohybrod employing chitosan/hydroxyethyl cellulose for controlled drug delivery. *Int. J. Pharmacol.* **2016**, 509, 400-407.

(44) Zhu, C., Liu, P., Mathew, A.P. Self-assembled TEMPO cellulose nanofibers: Graphene oxide-based biohybrids for water purification, *ACS App. Mat. Inter.* **2017**, 9, 21048-21058.

(45) Nada, A.A.M.A., Hassan, M.L. Phosphorylated cation-exchangers from cotton stalks and their constituents. *J. App. Poly. Sci.* **2003**, 89, 2950–2956.

(46) Yu, X., Tong, S., Ge, M., Wu, L., Zuo, J., Cao, C., Song, W. Adsorption of heavy metal ions from aqueous solution by carboxylated cellulose nanocrystals. *J. Environ. Sci.* **2013**, 25, 933–943.

(47) Tan, P., Sun, J., Hu, Y., Fang, Z., Bi, Q., Chen, Y., Cheng, J. Adsorption of Cu^{2+}, Cd^{2+} and Ni^{2+} from aqueous single metal solutions on grapheme oxide membranes. *J. Hazard. Mat.* **2015**, 302, 251–260.

(48) Setyono, D., Valiyaveettil, S. Functionalized paper a readily accessible ad-sorbent for removal of dissolved heavy metal salts and nanoparticles from water, *J. Hazard. Mat.* **2016**, 302, 120-128.

(49) Karim, Z., Afrin, S., Husian Q., Danish R. Necessity of enzymatic hydrolysis for production and functionalization of nanocelluloses. *Crit. Rev. Biotechnol.* **2017**, 37, 355-370.

(50) Karim, Z., Hakalahti, M., Tammelin, T., Mathew, A. P., Oksman, K. *In situ* TEMPO surface functionalization of nanocellulose membranes for enhanced adsorption of metal ions from aqueous medium. *RSC Advances,* **2017**, 7, 5232-5241.